Geophysical Prospecting, 2003, **51**, 99–115

PP amplitude bias caused by interface scattering: are diffracted waves guilty?

Nathalie Favretto-Cristini[1]* and Eric de Bazelaire[1,2]

[1]*Centre National de la Recherche Scientifique, Laboratoire d'Imagerie Géophysique UMR 5831, Université de Pau et des Pays de l'Adour, BP 1155-64013 Pau Cedex, and* [2]*TotalFinaElf, CSTJF, Avenue Larribau, 64018 Pau Cedex, France*

Received November 2000, revision accepted November 2002

ABSTRACT

This paper is concerned with the problem of interpretation of anomalous seismic amplitudes, induced by the amplitude-scattering phenomenon. This phenomenon occurs in the vicinity of a crack distribution at the interface between elastic layers. The purpose of this work is to obtain a better understanding of the physics of this distinctive phenomenon, in order to interpret correctly the amplitudes of the reflected events. By analogy with studies in optics and in acoustics, we suggest that diffraction is widely involved in the amplitude-scattering phenomenon. Analytical evaluation of the amount of energy carried by the reflected and the diffracted waves shows that neglecting diffraction in numerical models leads to local underestimation of the amplitude of waves reflected at interfaces with gas-filled crack distribution.

INTRODUCTION

One of the open issues for the geophysical community is amplitude-preserved imaging. Many geophysicists are interested in a better understanding and exploitation of true amplitudes in depth migration and amplitude versus offset (AVO) studies, in order to improve the estimation of the physical properties of geological structures (Tygel 2001). They concentrate mainly on the computation of the correct weight functions that are required in the Kirchhoff migration formalism. We address the issue of true amplitudes of seismic events, in certain geological contexts, from another viewpoint. Does elastic modelling really take into account all the physical mechanisms arising in media? If not, what are the effects of neglecting some physical phenomena?

The paper addresses the problem of interpretation of anomalous seismic amplitudes. The problem under consideration is shown in Figs 1 and 2.

Figure 1(a) illustrates a real data set recorded in the Niger Delta, while Fig. 1(b) represents data obtained by conventional, pure reflection modelling. Details of the velocities V_P and V_S and the density are known from several wells where gas was detected. In Fig. 1(a), some distinctive events arise at certain stratigraphic surfaces (transgressive and downward-shift surfaces), and only on the left of the fault. These real events have anomalous amplitudes compared with the corresponding impedance contrasts recorded in wells. The observed amplitudes are higher than expected from the reflection coefficient (Fig. 1b).

Figure 2 illustrates a walkaway imaging with wave arrivals at polarization angles of 0° to 90° with respect to a vertical well. Only the energy associated with P-waves has been represented in this figure. P–S wave conversions and very weak amplitudes of the reflected P-waves are noted essentially in two red areas in Fig. 2. These areas are water-saturated zones. The anomalous amplitudes of the P-waves in these areas can be compared with those of the P-waves transmitted through the saturated zones, with traveltimes of around 3.0 and 3.5 s.

In short, the real amplitudes of the reflected events are stronger (respectively, weaker) than expected when gas (respectively, liquid) was detected at some erosional surfaces in wells. Neither conventional, pure reflection modelling nor any modelling based on homogenization of the interface properties (Baik and Thompson 1984; Angel and Achenbach 1985; Nihei, Myer and Cook 1995; Liu, Hudson and Pointer

*E-mail: nathalie.favretto@univ-pau.fr

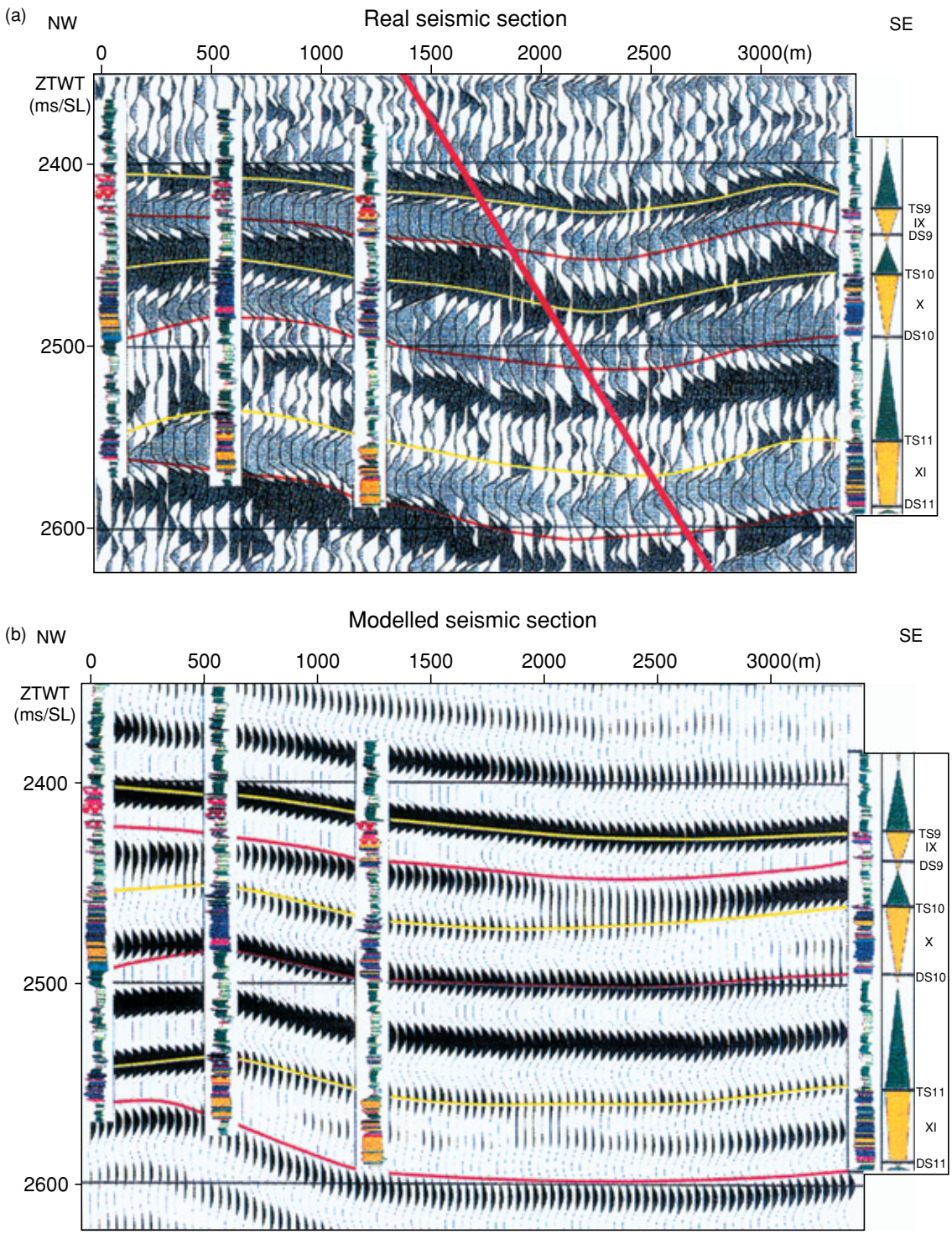

Figure 1 (a) An illustration of the 'gas amplitude-scattering' phenomenon on a real data set recorded in the Niger Delta. (b) Comparison with data obtained by pure reflection modelling. The log data are interpreted in terms of facies. The straight line represents a fault. (After Schulbaum 1996.)

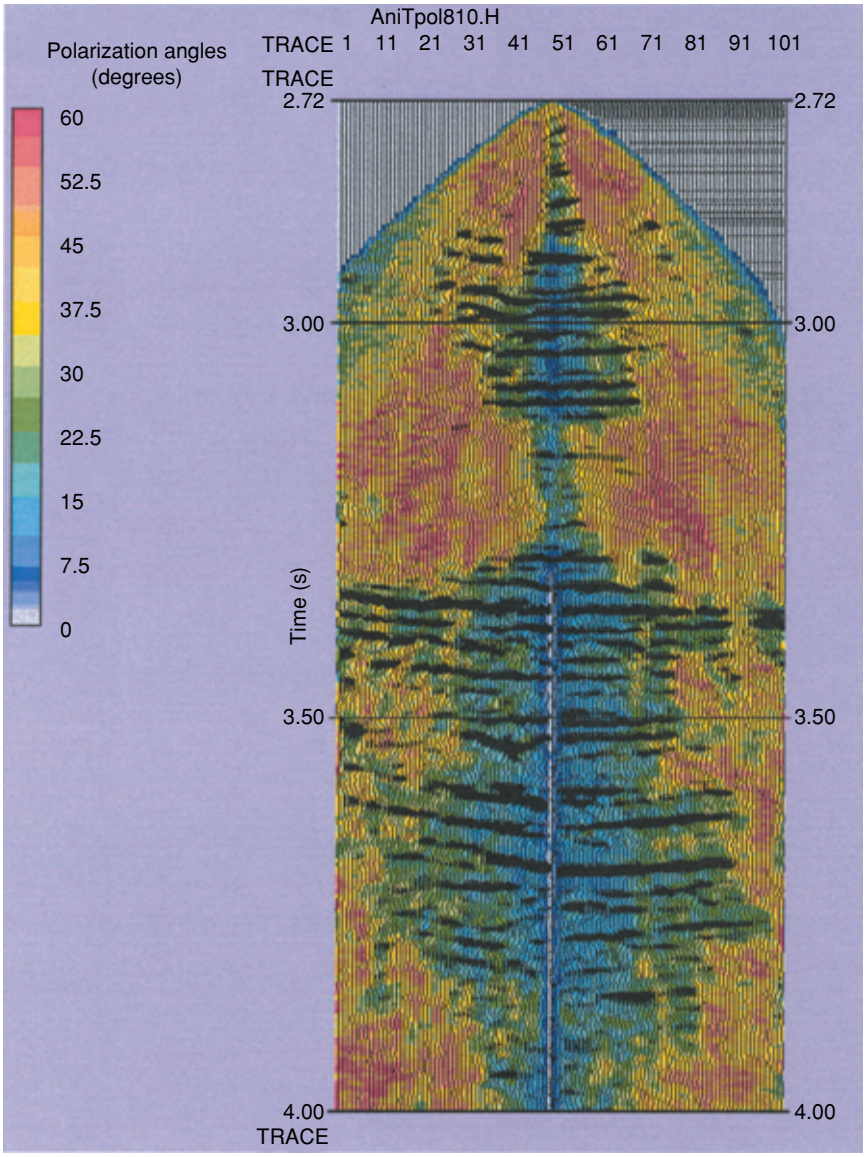

Figure 2 An illustration of the 'liquid amplitude-scattering' phenomenon on a walkaway imaging and polarization. Only the P-wave energy is represented. Blue areas represent P–P wave propagation, while red ones represent P–S wave conversions. (After J. Blanco 2000, pers. comm.)

2000; Myer 2000) could simulate these anomalous amplitudes. A phenomenon, different from pure reflection, was then neglected in such classical numerical models. We argue that the amplitude-scattering (AS) phenomenon is widely involved in such anomalous amplitudes. The aim of the paper is to show that neglecting such a distinctive phenomenon may lead to erroneous interpretation of real data in some cases, in particular when locating reflectors and inverting amplitudes.

The paper begins with a discussion of the AS phenomenon. What is it? Why can it not be modelled by classical numerical schemes? What are the physical mechanisms responsible for it? The second section briefly describes a way of modelling the AS phenomenon. Some numerical illustrations of the influence of the AS phenomenon on reflected events are also presented.

1 THE AMPLITUDE-SCATTERING (AS) PHENOMENON

In Fig. 1(a), events with anomalous amplitudes occur at certain stratigraphic surfaces. These surfaces result essentially from tectonics and/or erosion processes. These erosional surfaces are generally characterized by a spatial distribution of irregular geological contacts between layers. The cracks thus created at interfaces are filled with gas, liquid or solid. They

affect wave propagation, in particular elastic wave reflection, by creating interface scattering. At this point, we have to explain the meaning of the term 'interface scattering'. We consider interface scattering as scattering induced by a spatial distribution of irregular contacts between layers. Usually, both the phase and the amplitude of the incident wave may be altered by interface scattering on passing through the interface. In the special case when the amplitude but not the phase of the incident wavefront is altered, we speak of amplitude scattering, by analogy with optics (see Born and Wolf 1999, p. 447). If the phase but not the amplitude is altered, we speak of phase scattering. A well-known phase scatterer in land seismics is the weathered zone. More generally, interface roughnesses are phase scatterers whose effect on reflected signals has been studied extensively (Ogilvy 1991). Here, we are interested in the amplitude scattering induced by lateral heterogeneities at interfaces. We want to analyse the effects of a crack distribution at an interface on the amplitude of reflected signals. By analogy with studies in optics, in acoustics and in non-destructive testing (NDT) of materials, the spatial distribution of gas-, liquid- or solid-filled cracks may be viewed as diffraction gratings (Born and Wolf 1999). We consider that amplitude scattering results from the coherent or incoherent interference of the diffractions caused by each crack. Figures 1 and 2 clearly show that the effect of amplitude scattering on the amplitudes of reflected signals depends on the crack filling. We attempt to explain the physics behind these observations.

1.1 May interface waves (IW) be guilty?

The distribution of the welded contact areas and cracks between layers of a stratified earth can act as 'a comb transducer' (Viktorov 1967; Biryukov *et al.* 1995). The comb transducer is commonly used for excitation and detection of surface waves (Fig. 3). An incident P-wave, generated by an ultrasonic transducer, strikes the interface between the solid comb and the solid material. The P-wave is transformed into a surface wave (SW) at the end of the comb. The SW propagates at the free solid surface, and it is then coherently recombined by another comb into a P-wave. This P-wave is detected by another ultrasonic transducer. The incident wavelength determines the size of the active crack distribution.

We believe that such a physical mechanism can occur in the stratified earth, provided there is interaction between the incident wavelength and the spatial wavelength of the crack distribution. In future work, we will analyse in more detail the interference between the P-wave, resulting from the recombination of the SW by the crack distribution, and the bulk P-waves reflected at the interface.

1.2 May diffracted waves (DW) be guilty?

In order to understand better and to quantify the AS effects on seismic measurements, we consider a simple 2D propagation model, where the diffraction phenomena are clearly visible. Figure 4 depicts the 2D situation of two homogeneous elastic, isotropic half-spaces separated by a horizontal interface along which a periodic distribution of cracks exists. We refer to the lower medium as solid B and to the upper medium as solid A. We let K and Λ denote the spatial wavenumber and period of the crack distribution, with $K = 2\pi/\Lambda$. Figure 4 also indicates the distance between cracks, denoted by 2w. The quantity, $\Delta = Kw = \pi(2w/\Lambda)$, will be seen in the later derivations to be a useful parameter of the configuration.

We next consider an incident plane P-wave, characterized by wavelength λ_{inc} and time frequency ω, that propagates in solid B and strikes the interface below the incidence angle θ_{inc} with respect to the surface normal. The corresponding unit propagation vector is denoted $\mathbf{u}_{inc} = (\sin\theta_{inc}, \cos\theta_{inc})$.

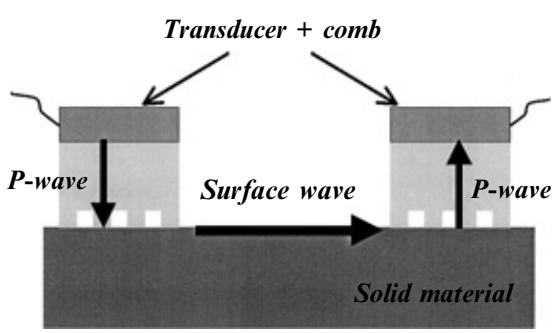

Figure 3 Excitation and detection of surface waves using comb transducers in acoustics and in NDT.

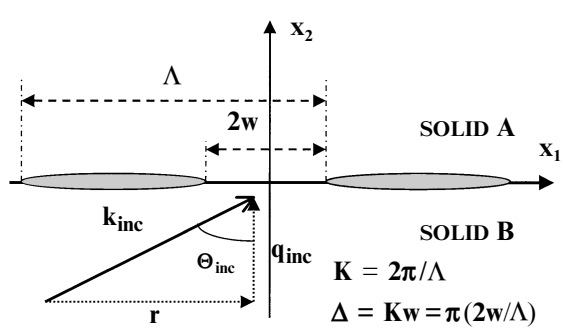

Figure 4 Periodic crack distribution at the boundary between Plexiglass® and Duraluminum® solids.

Finally, the wave vector of the incident wave is denoted $\mathbf{k}_{\text{inc}} = \boldsymbol{\omega}/\mathbf{s}_{\text{inc}} = (p_{\text{inc}}, q_{\text{inc}})$. Note that $\mathbf{s}_{\text{inc}} = (1/V_{\text{P}})\mathbf{u}_{\text{inc}}$ is the slowness vector of the incident wave, where V_{P} is the P-wave velocity of the lower half-space (solid B). Finally, we assume that the incident horizontal wavenumber p_{inc} satisfies the condition $p_{\text{inc}} = r$, with $0 < r < K$.

After striking the cracked interface, the incident plane wave excites many diffracted waves that propagate in different directions. Diffractions with diffraction order $n = 0$ correspond to specular P–P and P–S reflections and transmissions. Diffractions with diffraction order $n \neq 0$ correspond to non-specular reflections and transmissions, whose existence is due only to the presence of the crack distribution at the interface (see e.g. Waterman 1975; Danicki 1999). Diffraction is simply a generalization of reflection/transmission phenomena. As stated above, our aim is to understand better and to quantify the impact of the excited non-specular reflected and transmitted waves, compared with their specular counterparts, which are the only ones considered in seismic interpretations.

In the next section, we briefly indicate the wave propagation description from which the energy of the relevant reflected, transmitted and diffracted waves can be computed. However, in order to design the modelling parameters that are best suited to our needs, it is instructive to consider what is to be expected.

When $\Lambda \geq \lambda_{\text{inc}}$, where λ_{inc} denotes the incident wavelength and Λ denotes the spatial wavelength of the crack distribution, many diffracted waves in both media are propagative. For that reason, we consider the case $\Lambda = \lambda_{\text{inc}}$ as one of our modelling situations. The case $\Lambda \ll \lambda_{\text{inc}}$ is the usual assumption in most theories and in that situation, diffracted waves in both media are usually evanescent and, consequently, are neglected in models. However, when the properties of media in contact are very different, and under certain conditions on the ratio $\Lambda/\lambda_{\text{inc}}$, diffracted waves can be propagative. To check whether this is actually the case, we consider, as our second modelling example, the condition $\Lambda = (1/3)\lambda_{\text{inc}}$. The results can be illustrated graphically by means of wavevector diagrams, i.e. slowness diagrams drawn for the frequency $f = V_{\text{Pinc}}/\lambda_{\text{inc}}$ in Fig. 5. In such diagrams, the direction of wave propagation and the relationships between the angles of incidence, reflection and refraction are straightforward (see Crandall 1970; Fokkema 1980; Helbig 1994, p. 372).

The elastic parameters of the two half-spaces in Fig. 4 were chosen to be those of Plexiglass® (lower medium) and Duraluminum® (upper medium). The reason for the above choice is that these media will be used in future experiments under actual laboratory conditions. It should be noted that the properties of Plexiglass® and Duraluminum® are quite similar to those of chalk and granite.

Wavevector diagrams of the two examples under consideration, in which only propagative waves are represented, are shown in Fig. 5. In Fig. 5(a), the case $\Lambda = \lambda_{\text{inc}}$ is represented, while Fig. 5(b) depicts the corresponding diagram when $\Lambda = (1/3)\lambda_{\text{inc}}$. Note in both cases the four slowness circles

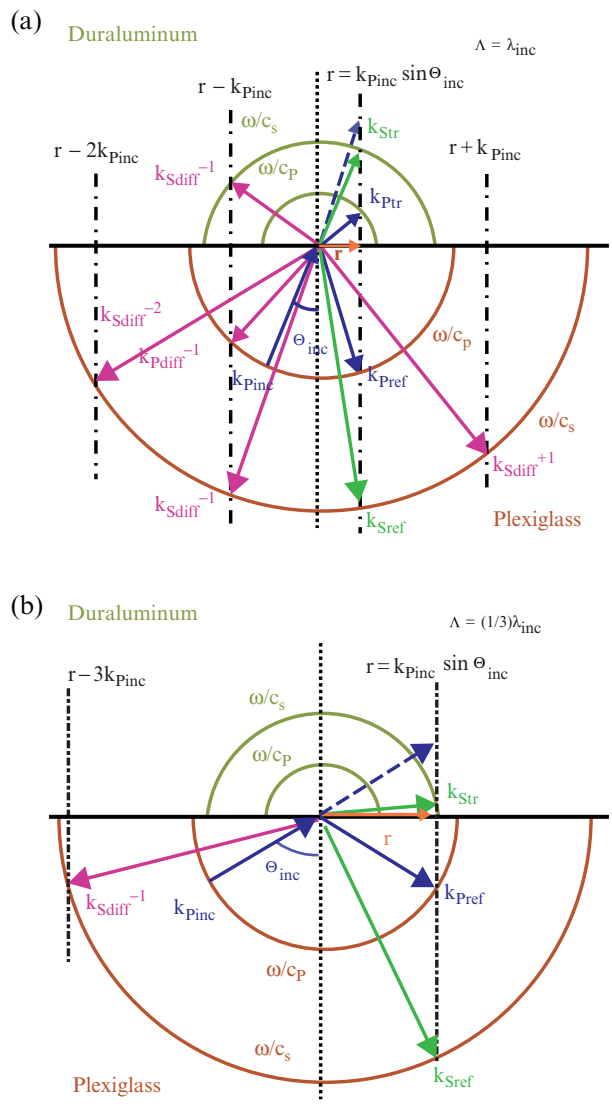

Figure 5 Wavevector diagrams illustrating diffraction (of order 0 and −1) of a P-wave incident on the Plexiglass®/Duraluminum® interface, for the cases (a) $\Lambda = \lambda_{\text{inc}}$ and (b) $\Lambda = (1/3)\lambda_{\text{inc}}$, Λ being the spatial wavelength of the gap distribution and λ_{inc} the incident P-wavelength. **k** is the wave vector. Only propagative waves are represented. The characteristics of the media are assumed to be: $V_{\text{P}} = 2670$ m/s and $V_{\text{S}} = 1120$ m/s (Plexiglass®), $V_{\text{P}} = 6440$ m/s and $V_{\text{S}} = 3170$ m/s (Duraluminum®).

for the given frequency f with radius $\omega/V_{P,S}$, where $V_{P,S}$ is the P- or S-wave velocity and $\omega = f/2\pi$ is the angular frequency. Following Brillouin and Parodi (1956), the wave vectors, $\mathbf{k}_{Pdiff}$ and $\mathbf{k}_{Sdiff}$, of the diffracted P- and S-waves are fixed by the requirement that their horizontal components, p_{Pdiff} and p_{Sdiff}, satisfy the condition $p_{Pdiff} = p_{Sdiff} = r + nK$, where n is an integer that characterizes the so-called diffraction order. The value $n = 0$ corresponds to the specular reflected and transmitted waves. Note that for $\Lambda < (1/3)\lambda_{inc}$, in the Plexiglass®/Duraluminum® configuration, only evanescent waves propagate at the interface, as the modulus of the horizontal components p_{Pdiff} and p_{Sdiff} of the wave vectors is such that $p_{P,Sdiff} = r \pm nK > k_{P,S}$.

1.3 The physical mechanisms involved in the AS phenomenon

As shown above, diffracted waves can arise from the crack distribution at the interface, provided there is interaction between the incident wavelength and the spatial wavelength of the crack distribution. In accordance with the energy conservation law, the energy carried by diffracted waves is not distributed to the other waves, in particular to the specular reflected P-waves. Neglecting diffraction phenomena, which is the case of interest here, leads to an incorrect energy balance, giving rise to an inaccurate estimation of the amplitudes of seismic reflections. As a consequence, the amplitudes of the specular reflected P-waves are generally overestimated in those numerical models that do not take into account the crack distribution at the interfaces. This is also true for the methods based on homogenization of the interface properties (Baik and Thompson 1984).

However, this result must be elaborated further, so as to take into account the situation in which the crack filling is either liquid or gas. The explanation is that the reflection coefficients in numerical models are calculated using only the impedances of the media in contact, without taking into account the crack distribution that produces diffraction effects. We consider such reflection coefficients as our reference reflection coefficients. The real reflection coefficient, 'measured' *in situ*, involves the effect of cracks. The real reflection coefficient is essentially a function of the impedance contrast between the crack filling and the first medium illuminated by the wave. The implicit condition is that the cracks are saturated. Consider first the case of water-saturated media in contact. The cracks at the interface are generally water-filled. The impedances of media and cracks are then quite similar. Replacing only the impedance of the medium into which waves are transmitted by the impedance of the crack filling does not modify the real reflection coefficient. Consequently, the amplitudes of the specular reflected P-waves are still overestimated in numerical models. Consider now the case of media in contact with gas-filled cracks. The impedances of media and cracks are very different, and the real reflection coefficient is greatly modified by this strong impedance contrast. The energy loss of the specular reflected P-waves, due to the presence of the diffracted waves, is then much weaker than the strong increase in the reflection coefficient. In this case, the amplitudes of the specular reflected P-waves may be underestimated in numerical models, as is shown in Fig. 1.

2 MODELLING OF THE AS PHENOMENON

It is clear that one of the key problems encountered in the modelling of the AS phenomenon is the difficulty in considering the crack distribution at interfaces in numerical schemes. Another difficulty is that of describing its effect on the wave propagation in the vicinity of the interface between layers. Previously, we suggested that the diffracted waves arising from the crack distribution were widely involved in the AS phenomenon. How can we model the diffraction effects? How can we quantify the diffracted and the specular reflected energies? How can we model the impact that the AS phenomenon has on seismic images? We propose to answer these questions by modelling the AS phenomenon in the simple 2D situation described in the previous section. As the present paper is concerned mainly with the interpretation of the modelling results and the relationship they have with conventional seismic interpretation, the analytical formulation of the wave-propagation problem will be presented briefly in the Appendix. Here, we give only the most relevant equations that are necessary for the calculations.

2.1 Numerical results

We are interested in the partitioning of the incident energy among the specular and non-specular reflected and transmitted waves in the solids A and B (see Fig. 4). The energy balance can be evaluated by determining the elastic Poynting vector, i.e. the time-averaged energy flux Π in the direction of $\boldsymbol{x}$, for each diffraction order n (Auld 1990):

$$\langle \mathbf{\Pi}_n^{A,B} \cdot \mathbf{x} \rangle = -\frac{1}{2}\Re\left(\mathbf{T}_n^{A,B^*} \cdot \left(j\omega \mathbf{U}_n^{A,B}\right) \cdot \mathbf{x}\right), \quad (1)$$

where the displacement vector $\mathbf{U}_n^{A,B}$ and the traction force vector $\mathbf{T}_n^{A,B}$ characterize the nth diffracted wavefield at the

interface (see Appendix), and the asterisk denotes complex-conjugate quantities. Usually, only the component Π_2 of Π along the $\mathbf{x}_2$-axis is considered in theoretical studies, as Π_2 is equal to zero for inhomogeneous waves that carry energy along the interfaces. However, rigorous characterization of the near-field wave propagation requires the evaluation of both components, Π_1 and Π_2, of the elastic Poynting vector. Here, we calculate only the component Π_2 associated with the specular ($n=0$) and non-specular ($n=-1$) reflected and transmitted P- and S-waves in each medium. With the help of (1) and (A4) (see Appendix), we find for $n=0$ (Danicki 1999):

$$\Pi_{\mathrm{P,S}}^{\mathrm{A,B}} = \frac{\rho_{\mathrm{A,B}}\omega^3}{2}\,\Re\left(\left|C_{\mathrm{P,S}}^{\mathrm{A,B}}\right|^2 q_{\mathrm{P,S}}^{\mathrm{A,B}}\right), \tag{2}$$

where the variables $C_{\mathrm{P,S}}^{\mathrm{A,B}}$ are expressed as a function of the traction force vector components

$$\begin{aligned}\begin{bmatrix} C_{\mathrm{P}}^{\mathrm{A}} \\ C_{\mathrm{S}}^{\mathrm{A}} \end{bmatrix} &= \frac{\mathrm{j}}{\mu_{\mathrm{A}} D_{\mathrm{A}}} \begin{bmatrix} 2p_n(q_{\mathrm{s}}^{\mathrm{A}})_n & k_{\mathrm{s}}^{\mathrm{A}^2} - 2p_n^2 \\ -(k_{\mathrm{s}}^{\mathrm{A}^2} - 2p_n^2) & 2p_n(q_{\mathrm{P}}^{\mathrm{A}})_n \end{bmatrix} \begin{bmatrix} (T_n^{\mathrm{A}})_1 \\ (T_n^{\mathrm{A}})_2 \end{bmatrix} \\ \begin{bmatrix} C_{\mathrm{P}}^{\mathrm{B}} \\ C_{\mathrm{S}}^{\mathrm{B}} \end{bmatrix} &= \frac{\mathrm{j}}{\mu_{\mathrm{B}} D_{\mathrm{B}}} \begin{bmatrix} 2p_n(q_{\mathrm{s}}^{\mathrm{B}})_n & -(k_{\mathrm{s}}^{\mathrm{B}^2} - 2p_n^2) \\ k_{\mathrm{s}}^{\mathrm{B}^2} - 2p_n^2 & 2p_n(q_{\mathrm{P}}^{\mathrm{B}})_n \end{bmatrix} \begin{bmatrix} (T_n^{\mathrm{B}})_1 \\ (T_n^{\mathrm{B}})_2 \end{bmatrix}. \end{aligned} \tag{3}$$

The energy conservation law implies that

$$\sum_n \left\langle \mathbf{\Pi}_n^{\mathrm{A,B}} \cdot \mathbf{x}_2 \right\rangle = \langle \mathbf{\Pi}_{\mathrm{inc}} \cdot \mathbf{x}_2 \rangle, \tag{4}$$

that is, for $n=0$:

$$\langle \mathbf{\Pi}_{\mathrm{inc}} \cdot \mathbf{x}_2 \rangle = \Pi_{\mathrm{P}}^{\mathrm{A}} + \Pi_{\mathrm{S}}^{\mathrm{A}} + \Pi_{\mathrm{P}}^{\mathrm{B}} + \Pi_{\mathrm{S}}^{\mathrm{B}}, \tag{5}$$

and for $n \neq 0$ (here, $n=-1$)

$$\begin{aligned}\langle \mathbf{\Pi}_{\mathrm{inc}} \cdot \mathbf{x}_2 \rangle = &\left(\Pi_{\mathrm{P}}^{\mathrm{A}} + \Pi_{\mathrm{S}}^{\mathrm{A}} + \Pi_{\mathrm{P}}^{\mathrm{B}} + \Pi_{\mathrm{S}}^{\mathrm{B}}\right) \\ &+ \left(\Pi_{\mathrm{Pdiff}}^{\mathrm{A}} + \Pi_{\mathrm{Sdiff}}^{\mathrm{A}} + \Pi_{\mathrm{Pdiff}}^{\mathrm{B}} + \Pi_{\mathrm{Sdiff}}^{\mathrm{B}}\right). \end{aligned} \tag{6}$$

Π_{inc} is the time-averaged energy flux associated with the incident wave.

Figures 6, 7, 8 and 9 illustrate the changes in the calculated ratio of the energy scattered by the P- and S-waves in the Plexiglass® and Duraluminum® solids to the incident energy, i.e. $\langle \mathbf{\Pi}_{\mathrm{P,S}}^{\mathrm{A,B}} \cdot \mathbf{x}_2 \rangle / \langle \mathbf{\Pi}_{\mathrm{inc}} \cdot \mathbf{x}_2 \rangle$ for $n=0$ and $\langle \mathbf{\Pi}_{\mathrm{P,Sdiff}}^{\mathrm{A,B}} \cdot \mathbf{x}_2 \rangle / \langle \mathbf{\Pi}_{\mathrm{inc}} \cdot \mathbf{x}_2 \rangle$ for $n=-1$, as a function of the incidence angle Θ_{inc}. The influence of the ratio $2\mathrm{w}/\Lambda$ (see Fig. 4) on the energy scattered is also shown. The ratio $2\mathrm{w}/\Lambda = 0.01$ represents the case in which the interface is almost completely disbonded, and the ratio $2\mathrm{w}/\Lambda = 0.99$ represents the case of a quasi-perfectly welded interface, hereafter referred to as the reference case. The incident P-wavelength λ_{inc} in Plexiglass® is greater than the spatial wavelength Λ of the crack distribution at the interface ($\Lambda = (1/3)\lambda_{\mathrm{inc}}$).

In Figs 6, 7, 8 and 9, we can observe the different critical angles corresponding to the refraction, along the interface, of the P- and S-waves in Duraluminum®:

$\Theta_{\mathrm{PDural}} = \arcsin(V_{\mathrm{PPlexi}}/V_{\mathrm{PDural}}) = 25^\circ$,

$\Theta_{\mathrm{SDural}} = \arcsin(V_{\mathrm{PPlexi}}/V_{\mathrm{SDural}}) = 57^\circ$.

For $\Lambda = (1/3)\lambda_{\mathrm{inc}}$, the diffracted S-wave of order -1 is propagative for the incident angles $\Theta_{\mathrm{inc}} > 38^\circ$. For $\Theta_{\mathrm{inc}} < 38^\circ$, the sum of the reflected and transmitted energy must be unity. This is not perfectly true in Figs 6(a), 7(a), 8(a) and 9(a), because the number of space harmonics retained in the field expansion (see Appendix), that determines the accuracy of the amplitude of the individual diffracted orders, was intentionally taken small, for simplicity of calculation. Above 38°, the diffracted energy must be taken into account in the energy balance. In Fig. 6(a), a Rayleigh wave that propagates at the free surface of the Duraluminum® material is generated at the incident angle $\Theta_{\mathrm{inc}} = 64^\circ$. This result appears consistent with the assumption of Section 1.1, that the crack distribution at the interface acts as a 'comb transducer'. The most important and new result, illustrated in Figs 6, 7 and 8, is the evaluation of the amount of energy associated with the diffracted wave. For the case of the quasi-disbonded interface, i.e. for $2\mathrm{w}/\Lambda = 0.01$ and for $2\mathrm{w}/\Lambda = 0.5$, the amount of energy is on average about 15% (Figs 6b and 7b). This amount decreases with increasing ratios, $2\mathrm{w}/\Lambda = 0.75$ and $2\mathrm{w}/\Lambda = 0.99$. For the reference case, the amount of energy is equal to zero, as no diffracted wave is generated (Fig. 9b). These results confirm the statement that neglecting the crack distribution at the interface, and the diffracted waves arising from this diffraction grating, leads to overestimation of the amplitude of the reflected events. In the case of the quasi-disbonded interface, i.e. for $2\mathrm{w}/\Lambda = 0.01$, the amplitude of the reflected P-wave is higher than its counterpart in the reference case, as the incident P-wave is fully reflected by the interface (Fig. 6a).

It should be noted that the curve describing the variation of the reflected P-wave energy for the incident angle $\Theta_{\mathrm{inc}} < 25^\circ$ is similar to that obtained in classical amplitude versus angle (AVA) images. For a weak impedance contrast between materials, the critical angle is generally about 70°.

2.2 Modelling of seismic images

The purpose of this section is to illustrate the consequences of the previous theoretical results on seismic images.

Figures 10, 11, 12 and 13 show the modelling of the reflected P-wave AVO in the Plexiglass®/Duraluminum® configuration. Figures 10(a), 11(a), 12(a) and 13(a) represent the

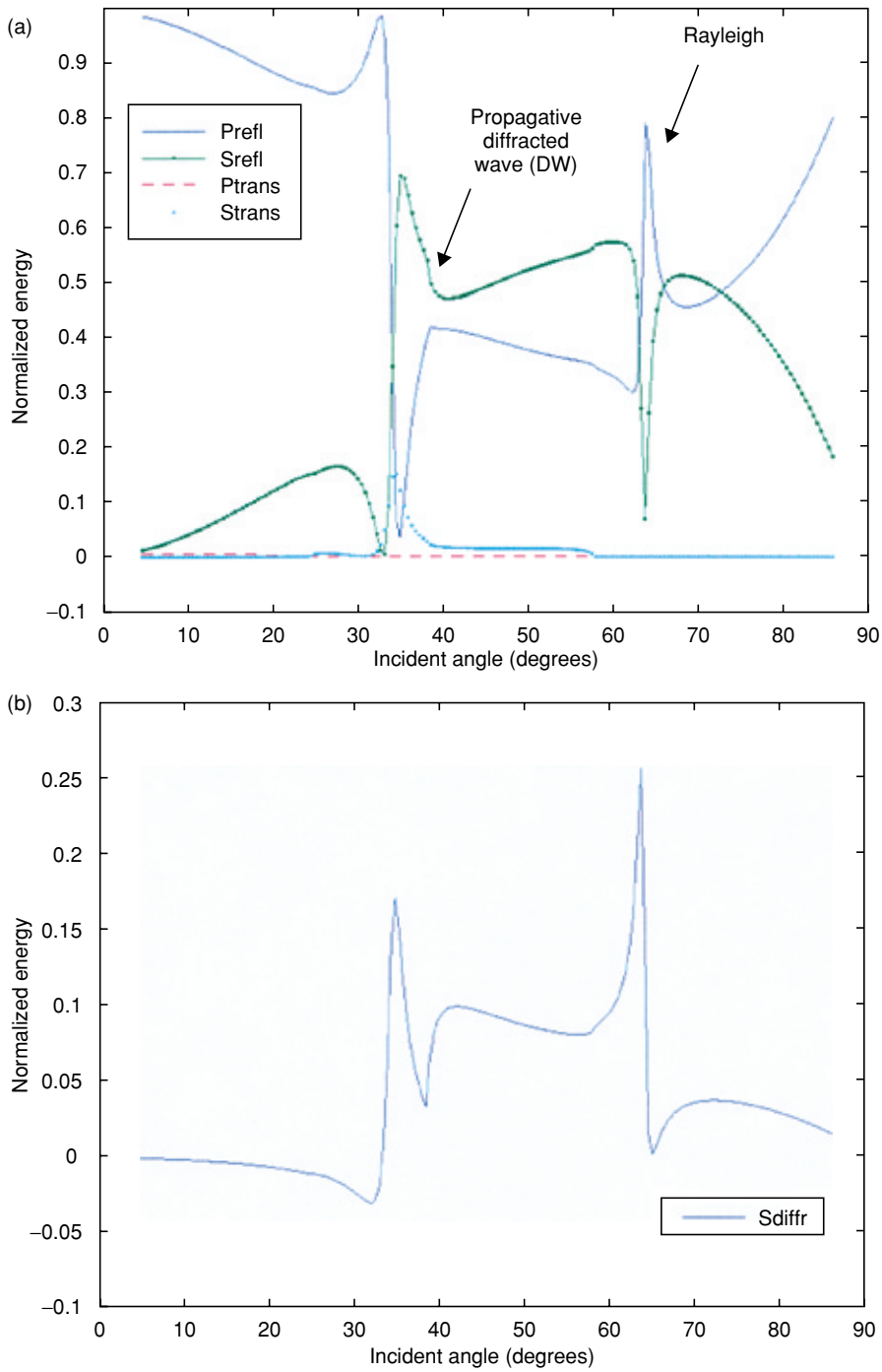

Figure 6 Energy of (a) the reflected and transmitted P- and S-waves, and (b) the diffracted S-wave as a function of the incident angle Θ_{inc}, in the Plexiglass®/Duraluminum® configuration. The characteristics of the gap distribution at the interface are: $\Lambda = (1/3)\lambda_{inc}$ and $2w/\Lambda = 0.01$.

AVO in 3D and Figs 10(b), 11(b), 12(b) and 13(b) represent the synthetic seismograms. The amplitude is calculated, for different crack distribution properties, from the theoretical analysis described in the previous section, by considering the CMP gather in a horizontal layer of thickness 1000 m and with P-wave velocity of 2670 m/s. The source signal (second-order Ricker) is modulated in AVO by the square root of the P-wave energy calculated analytically. The CMP gather is

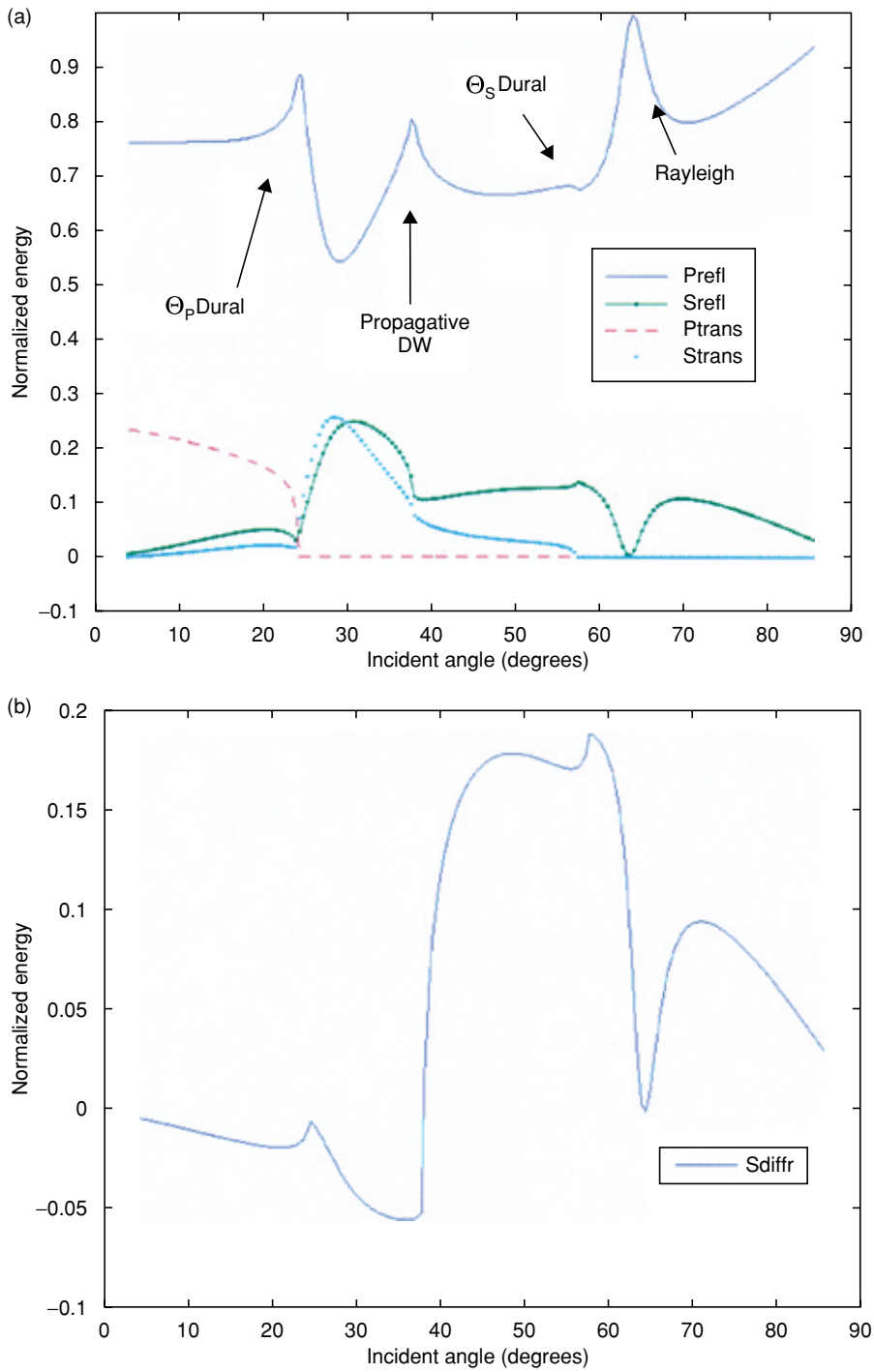

Figure 7 As Fig. 6 with the characteristic $2w/\Lambda = 0.5$.

assumed to have been processed with dynamic correction and geometrical amplitude compensation. As previously, Fig. 10 corresponds to the almost completely disbonded interface and Fig. 13 to the welded interface (reference image).

First, compare the traces corresponding to a small aperture (i.e. $0 < \Theta_{inc} < 38°$). The reflected P-wave stacking energy increases with decreasing ratio $2w/\Lambda$, which agrees with the usual theoretical considerations. For these small offsets, a theory

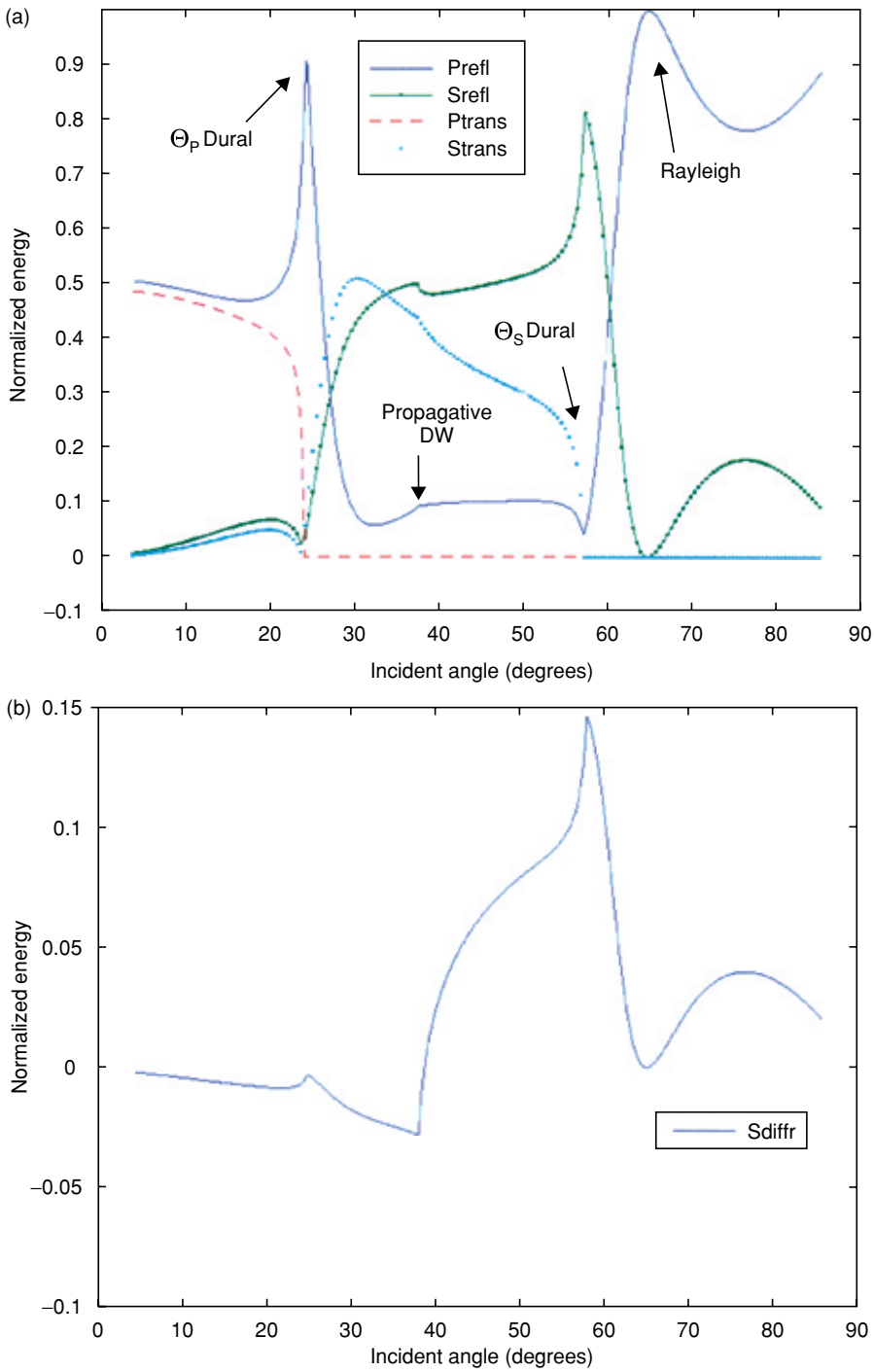

Figure 8 As Fig. 6 with the characteristic $2w/\Lambda = 0.75$.

based on homogenization of the interface properties can describe very well the behaviour of the real physical mechanisms, as no diffraction phenomena are involved. By contrast, for a greater aperture (say, $0 < \Theta_{inc} < 60°$), diffraction phenomena are involved in the far traces ($38° < \Theta_{inc} < 60°$), and homogenization of the interface properties can no longer be applied. In this case, classical numerical models that do not take diffraction phenomena into account underestimate the amplitude of

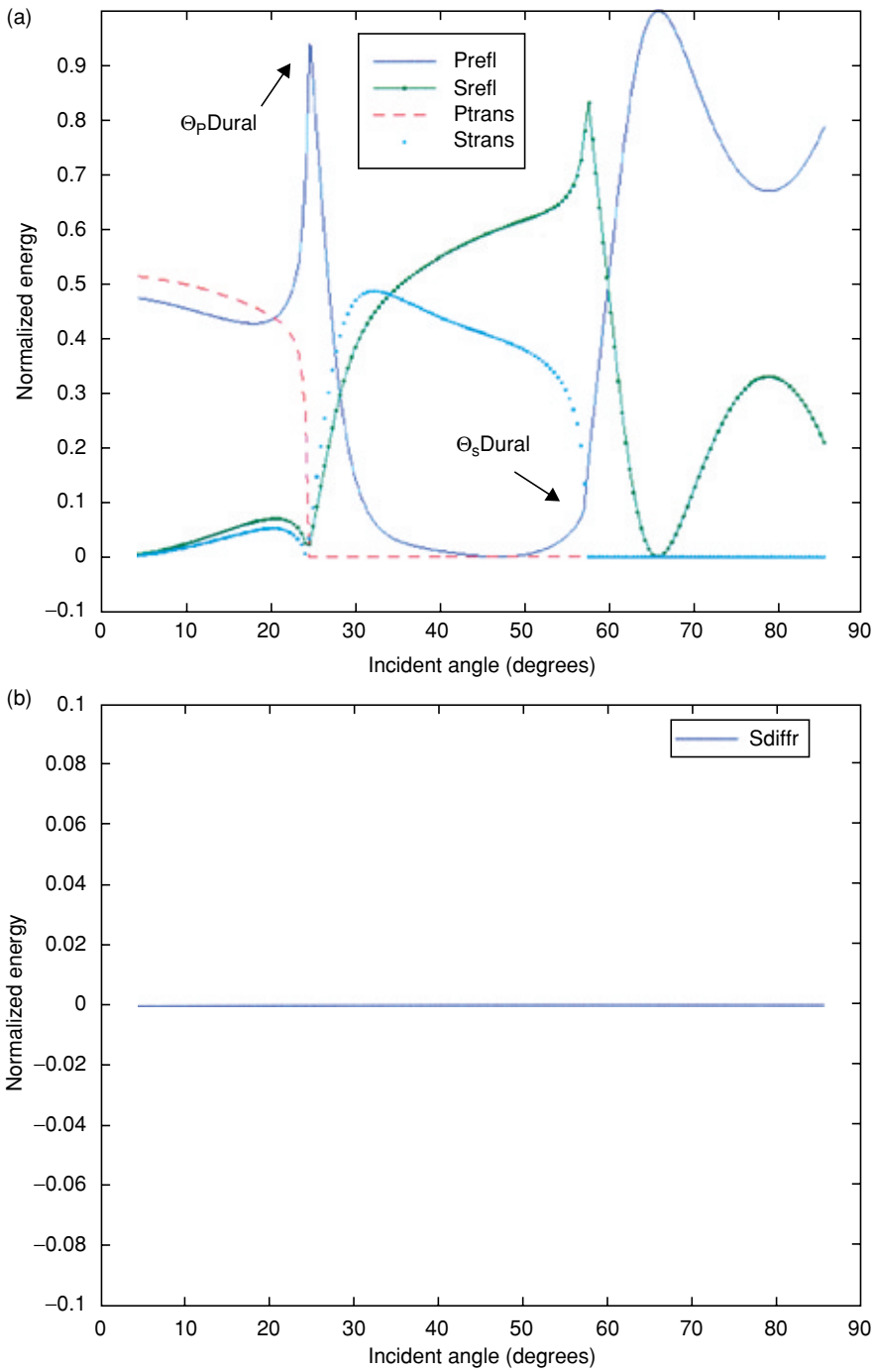

Figure 9 As Fig. 6 with the characteristic $2w/\Lambda = 0.99$.

the reflected P-wave, as is suggested by comparison of the traces in Figs 10(b) and 13(b). These results appear consistent with the discussion in Section 1.3 and with Fig. 1. Finally, let us examine the amount of the reflected P-wave energy in the far traces ($38^\circ < \Theta_{inc} < 60^\circ$) in Figs 10(b)–13(b). The amount of energy initially increases with decreasing ratio $2w/\Lambda$, reaching a maximum value for $2w/\Lambda = 0.5$; it then decreases with decreasing ratio $2w/\Lambda$. At the moment we do not have a full explanation for these striking characteristics, also observed in Figs 6(a)–9(a). They will be analysed in future work.

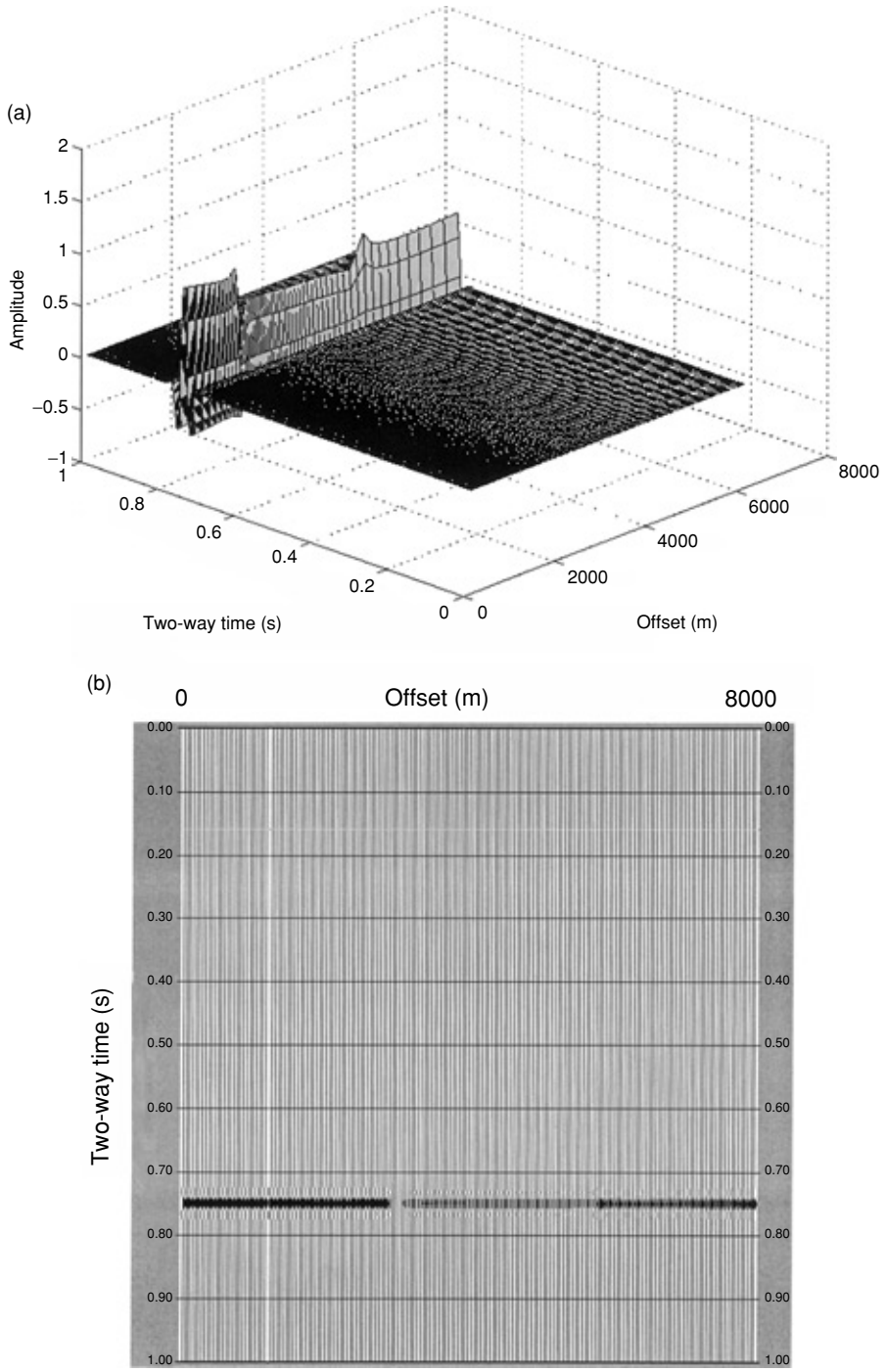

Figure 10 Modelling of the reflected P-wave AVO in the Plexiglass®/Duraluminum® configuration. (a) AVO in 3D; (b) synthetic seismograms. The characteristics of the gap distribution at the interface are: $\Lambda = (1/3)\lambda_{inc}$ and $2w/\Lambda = 0.01$.

CONCLUSION

This study was concerned with the problem of interpretation of anomalous seismic amplitudes induced by the amplitude-scattering (AS) phenomenon. This phenomenon, which alters the amplitude of the incident wavefronts, results from coherent and incoherent interference of diffractions caused by each element of a crack distribution at the interface between elastic layers.

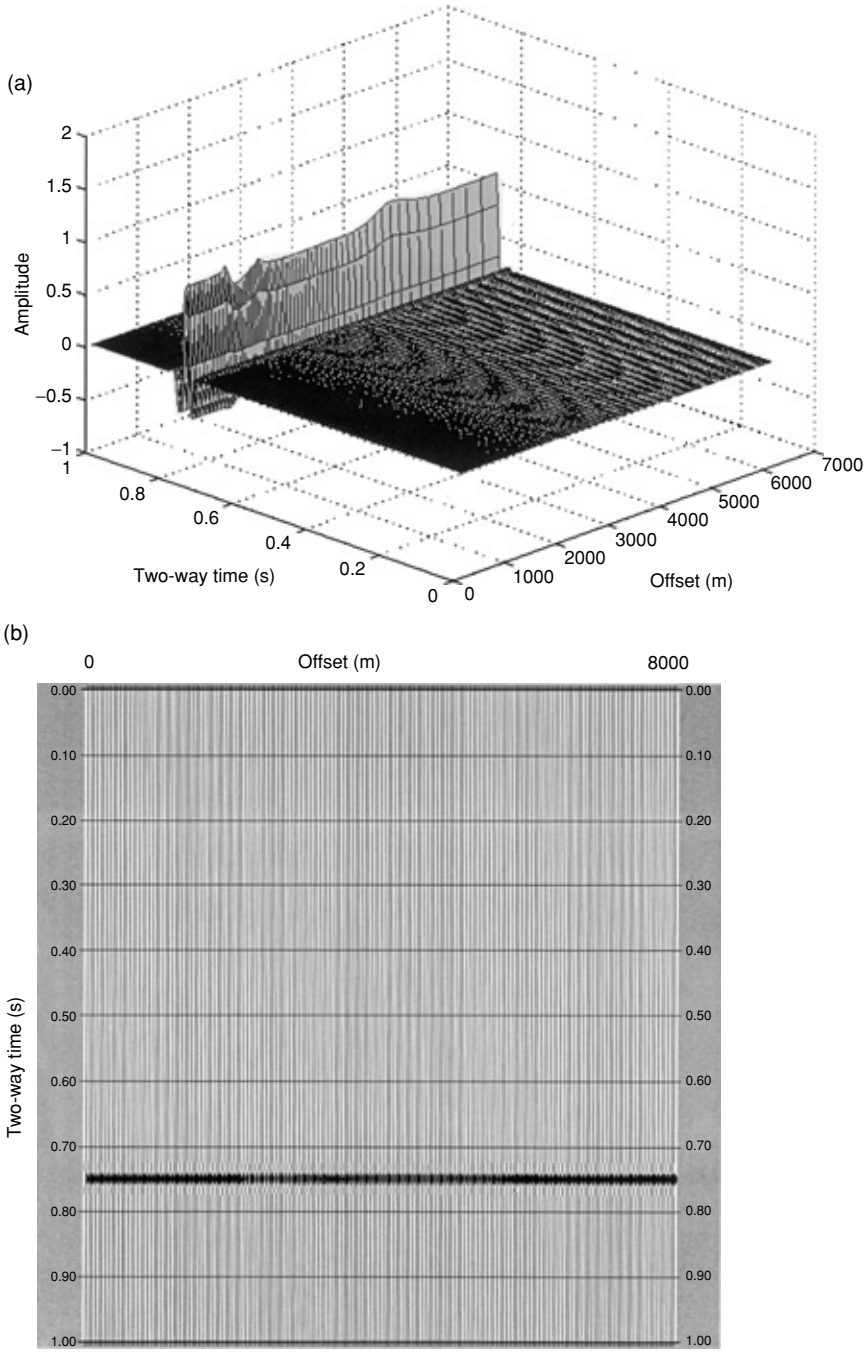

Figure 11 As Fig. 10 with the characteristic $2w/\Lambda = 0.5$.

Analysis of real seismic data has suggested that the effect of AS on the amplitudes of reflected signals depends on the crack filling (gas or liquid). The aim of the paper was to obtain a better understanding of the physics behind these observations.

Analogy with studies in optics, in non-destructive testing and in acoustics has suggested that diffraction phenomena arising from the crack distribution are widely involved in the anomalous amplitudes of reflected events. Analytical evaluation of the amount of energy carried by the reflected and the diffracted waves has shown that neglecting diffraction phenomena leads to local underestimation of the amplitude of waves reflected at interfaces with gas-filled cracks.

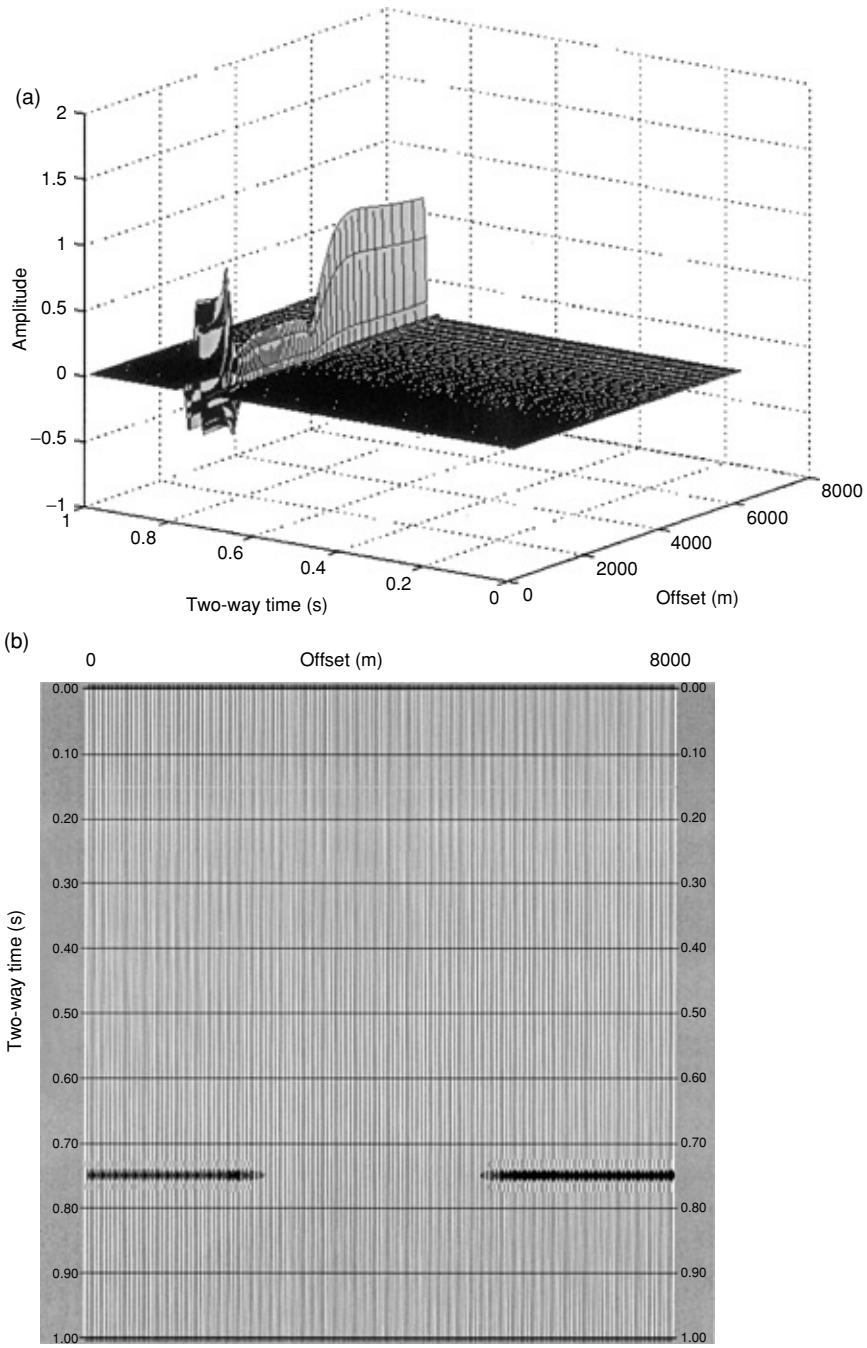

Figure 12 As Fig. 10 with the characteristic $2w/\Lambda = 0.75$.

Consequently, classical numerical modelling of seismic data that do not take into account diffraction phenomena cannot simulate correctly the real data amplitudes.

The influence of the AS phenomenon on seismic waves reflected at interfaces with liquid-filled cracks will be analysed in a forthcoming paper.

ACKNOWLEDGEMENTS

Martin Tygel showed much interest in this study. We thank him for his pertinent remarks and review that helped us to clarify many important points. Thanks to Hervé Perroud for reviewing an earlier version of the manuscript

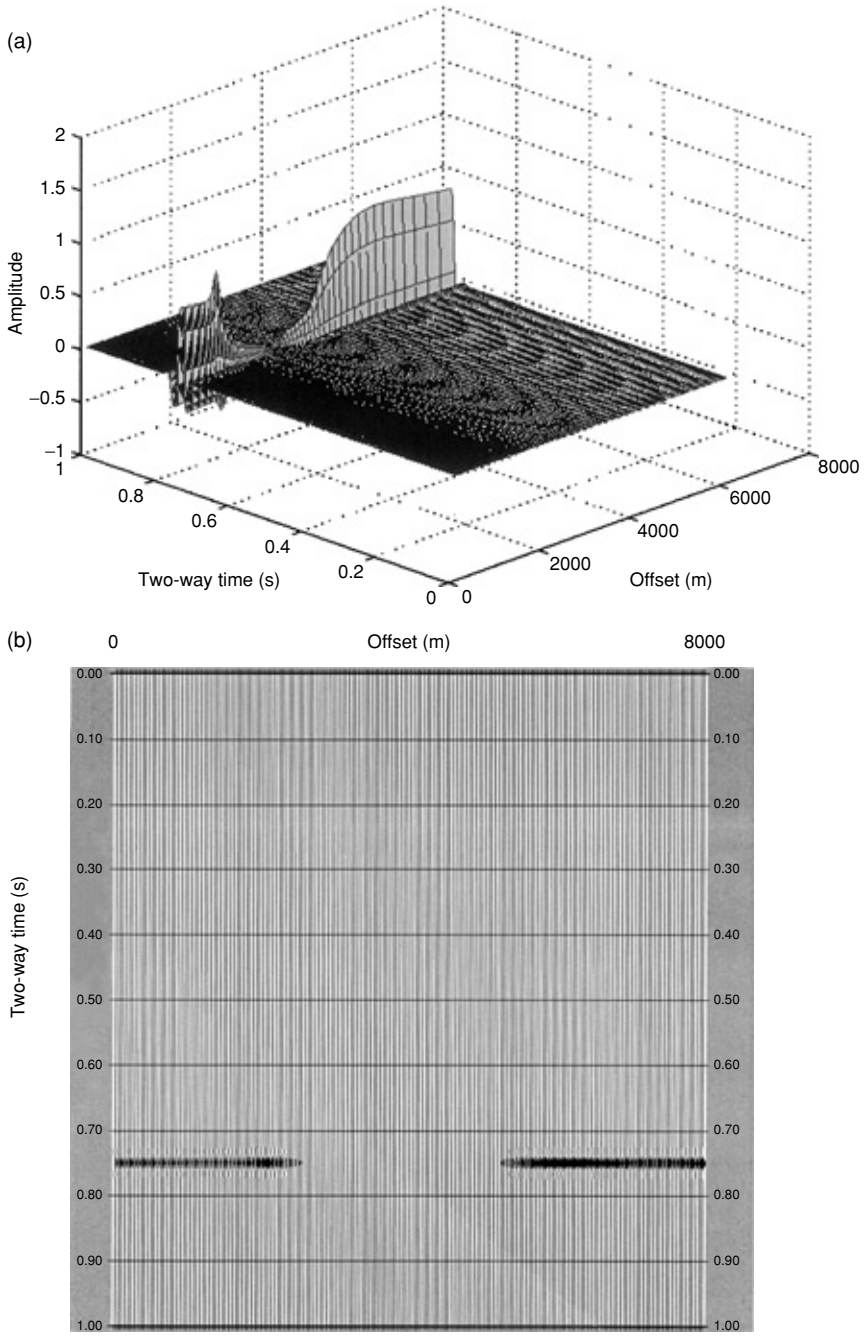

Figure 13 As Fig. 10 with the characteristic $2w/\Lambda = 0.99$.

and to Evgeny Landa for his encouragement. We are also grateful to Jacques Blanco and Laurent Schulbaum for providing the real seismic sections, and to Jean Magendie and Didier Rappin for providing the synthetic seismograms.

REFERENCES

Angel Y.C. and Achenbach J.D. 1985. Reflection of ultrasonic waves by an array of cracks. In: *Review of Progress in Quantitative Nondestructive Evaluation 4A* (eds D.O. Thompson and D.E. Chimenti), pp. 83–89. Plenum Press.

Auld B.A. 1990. *Acoustic Fields and Waves in Solids*, 2nd edn, two volumes. Krieger Publishing Co.

Baik J.-M. and Thompson R.B. 1984. Ultrasonic scattering from imperfect interfaces: a quasi-static model. *Journal of Nondestructive Evaluation* **4**(3/4), 177–196.

Biryukov S.V., Gulyaev Yu.V., Krylov V.V. and Plessky V.P. 1995. *Surface Acoustic Waves in Inhomogeneous Media* (eds L.M. Brekhovskikh *et al.*). Springer-Verlag, Inc.

Born M. and Wolf E. 1999. *Principles of Optics*, 7th expanded edn. Cambridge University Press.

Brillouin L. and Parodi M. 1956. *Propagation des Ondes dans les Milieux Périodiques*. Masson et Cie, Paris.

Crandall S.H. 1970. On the use of slowness diagrams to represent wave reflections. *Journal of the Acoustical Society of America* **47**, 1338–1342.

Danicki E. 1999. Resonant phenomena in bulk wave scattering by in-plane cracks. *Journal of the Acoustical Society of America* **105**, 84–92.

Fokkema J.T. 1980. Reflection and transmission of elastic waves by the spatially periodic interface between two solids (theory of the integral-equation method). *Wave Motion* **2**, 375–393.

Helbig K. 1994. *Foundations of Anisotropy for Exploration Seismics. Handbook of Geophysical Exploration, Section 1: Seismic Exploration*, **Vol. 22** (eds K. Helbig and S. Treitel). Pergamon Press, Inc.

Liu E., Hudson J.A. and Pointer T. 2000. Equivalent medium representation of fractured rock. *Journal of Geophysical Research* **105** (B2), 2981–3000.

Myer L.R. 2000. Fracture as a collection of cracks. *International Journal of Rock Mechanics and Minerals Science* **37**, 231–242.

Nihei K.T., Myer L.R. and Cook N.G.W. 1995. Numerical simulation of elastic wave propagation in granular rock with the boundary integral equation method. *Journal of the Acoustical Society of America* **97**, 1423–1434.

Ogilvy J.A. 1991. *Theory of Wave Scattering from Random Rough Surfaces*. Hilger.

Schulbaum L. 1996. *Traduction des surfaces stratigraphiques et des géométries deltaïques lors du passage de l'échelle puits à l'échelle sismique*. PhD thesis, Henri Poincaré Nancy I University.

Tygel M. (ed.) 2001. Special issue: Seismic true amplitudes. *Journal of Seismic Exploration* **10**.

Viktorov I.A. 1967. *Rayleigh and Lamb Waves* (ed. W.P. Mason). Plenum Press.

Waterman P.C. 1975. Scattering by periodic surfaces. *Journal of the Acoustical Society of America* **57**, 791–802.

APPENDIX

We derive expressions for the diffracted wavefield induced by a crack distribution at the interface between two different solids. These expressions are necessary for the evaluation of the amount of energy carried by each diffracted wave (see Section 2.1).

As described in Section 1.2, we consider a time-harmonic plane P-wave propagating in the solid B, at an angle Θ_{inc} with respect to the normal to the solid B/solid A interface, towards the solid A (Fig. 4). The associated incident displacement vector $\mathbf{U}_{\text{inc}}$ in the solid B can be written as

$$\mathbf{U}_{\text{inc}}(x_1, x_2; t) = \mathbf{u}_{\text{inc}}(x_1, x_2)\exp(-\mathrm{j}q_{\text{inc}}x_2)\exp(-\mathrm{j}p_{\text{inc}}x_1)\exp(\mathrm{j}\omega t),$$

where $\mathbf{u}_{\text{inc}} = (\sin\mathbf{\Theta}_{\text{inc}}, \cos\mathbf{\Theta}_{\text{inc}})$ is the unit propagation vector of the incident P-wave, $\mathbf{k}_{\text{inc}} = (p_{\text{inc}}, q_{\text{inc}}) = \mathbf{k}_{\text{P}}^{\text{B}}$ is the incident P-wavenumber and ω is the angular frequency.

At the interface, the full wavefield (displacement $\mathbf{U}_{\text{tot}}^{\text{A,B}}$ and stress $\mathbf{T}_{\text{tot}}^{\text{A,B}}$) in each medium, governed by known equations of motion, is expressed in the form:

In the solid A:

$$\begin{cases} \mathbf{U}_{\text{tot}}^{\text{A}} = \mathbf{U}_{\text{diff}}^{\text{A}} \\ \mathbf{T}_{\text{tot}}^{\text{A}} = \mathbf{T}_{\text{diff}}^{\text{A}} \end{cases}, \tag{A1}$$

and in the solid B:

$$\begin{cases} \mathbf{U}_{\text{tot}}^{\text{B}} = \mathbf{U}_{\text{inc}} + \mathbf{U}_{\text{diff}}^{\text{B}} \\ \mathbf{T}_{\text{tot}}^{\text{B}} = \mathbf{T}_{\text{inc}} + \mathbf{T}_{\text{diff}}^{\text{B}} \end{cases}. \tag{A2}$$

$\mathbf{U}_{\text{diff}}^{\text{A,B}}$ and $\mathbf{T}_{\text{diff}}^{\text{A,B}}$ characterize the diffracted fields in the solids A and B. At the interface, they are formulated as an infinite series of Bloch waves, as required by Floquet's theorem (see Waterman 1975; Auld 1990, vol. 2, p. 119):

$$\begin{bmatrix} \mathbf{T}_{\text{diff}}^{\text{A,B}} \\ \mathbf{U}_{\text{diff}}^{\text{A,B}} \end{bmatrix} = \sum_{n=-\infty}^{+\infty} \begin{bmatrix} \mathbf{T}_n^{\text{A,B}} \\ \mathbf{U}_n^{\text{A,B}} \end{bmatrix} \exp(-\mathrm{j}p_n x_1)\exp(\mathrm{j}\omega t), \tag{A3}$$

where $p_n = p_{\text{inc}} + nK$ is the Bloch wavenumber, n is the diffraction order and $K = 2\pi/\Lambda$ is the spatial wavenumber of the crack distribution defined from the spatial wavelength Λ. The diffracted fields represent the specular ($n = 0$) and non-specular ($n \neq 0$) reflected and transmitted fields. The wavefield in each medium is a superposition of the diffracted P- and S-waves components, with the general form,

$$\exp(-\mathrm{j}p_n x_1)\exp\left(\pm\mathrm{j}\left(q_{\text{P,S}}^{\text{A,B}}\right)_n x_2\right)\exp(\mathrm{j}\omega t),$$

where

$$\left(q_{\text{P,S}}^{\text{A,B}}\right)_n = \left(k_{\text{P,S}}^{\text{A,B}^2} - p_n^2\right)^{1/2} = -\mathrm{j}\left(p_n^2 - k_{\text{P,S}}^{\text{A,B}^2}\right)^{1/2}$$

with P- and S-wavenumbers $k_{\text{P,S}}^{\text{A,B}}$.

At the interface, the coefficients $\mathbf{U}_n^{\text{A,B}}$ and $\mathbf{T}_n^{\text{A,B}}$ of the infinite series, and the incident displacement $\mathbf{U}_{\text{inc}}$ and traction-force $\mathbf{T}_{\text{inc}}$ vectors (Auld 1990), are related by

$$\mathbf{U}_n^{\text{A,B}} = \overline{\overline{\mathbf{G}_n^{\text{A,B}}}}\,\mathbf{T}_n^{\text{A,B}},\ \mathbf{U}_{\text{inc}} = \overline{\overline{\mathbf{G}'_{\text{inc}}}}\,\mathbf{T}_{\text{inc}}, \tag{A4}$$

where the matrices $\overline{\overline{\mathbf{G}_n^{\text{A,B}}}}$ and $\overline{\overline{\mathbf{G}'_{\text{inc}}}}$ are defined from the known equations of motion.

The full wavefields ($\mathbf{U}_{\text{tot}}^{\text{A,B}}$ and $\mathbf{T}_{\text{tot}}^{\text{A,B}}$) must satisfy different boundary conditions at the interface:
on cracks

$$\mathbf{T}_{\text{tot}}^{\text{A}} = \mathbf{T}_{\text{tot}}^{\text{B}} = \mathbf{0}, \tag{A5a}$$

between cracks

$$\begin{cases} \Delta\mathbf{U} = \mathbf{U}_{\text{diff}}^{\text{A}} - \mathbf{U}_{\text{diff}}^{\text{B}} = \mathbf{0} \\ \mathbf{T}_{\text{tot}}^{\text{A}} = \mathbf{T}_{\text{tot}}^{\text{B}} \end{cases}, \tag{A5b}$$

where the function $\Delta\mathbf{U}$ denotes the particle displacement discontinuity at the interface. These boundary conditions cannot be exploited in a trivial way to analyse the wave diffraction problem. An efficient way of solving such a problem can be found in Danicki (1999). The paper presents a method of analysis of the generation of surface waves by comb transducers. This work is concerned with a crack distribution embedded in an isotropic elastic body. As the objectives of our work are different, we need to derive equations for the case of two different elastic media in contact. We then adapted the original work to our configuration. Referring the reader for details to the original paper (Danicki 1999), we give only the most relevant equations that are necessary for our work. Danicki (1999) assumed a finite series expansion for $\mathbf{T}_n^{\text{A}}$ in the form,

$$\mathbf{T}_n^{\text{A}} = \sum_{m=N_1}^{N_2+1} \mathbf{t}_{nm}^{\text{A}} P_{n-m}(\cos\Delta), \tag{A6}$$

in which P_n denotes Legendre functions of the first kind, and the variable $\Delta = K\text{w}$ describes the relative width of perfect contact between cracks (Fig. 4). Some interesting properties of Legendre functions allow the diffracted fields to satisfy the boundary conditions and the square-root singularities at the crack edges.

After some long but straightforward calculations (see Danicki 1999), analysis of the wave diffraction by periodic systems of in-plane cracks can be achieved by solving the system of $(N_2 - N_1 + 2)$ equations in $(N_2 - N_1 + 2)$ unknowns $\mathbf{t}_{nm}^{\text{A}}$, resulting from the boundary conditions (A5):

$$\begin{cases} \sum_{m=N_1}^{N_2+1} \left(S_{n-m}\,\overline{\overline{\mathbf{g}_\infty^n}} - \overline{\overline{\mathbf{g}_n}}\right)\mathbf{t}_{nm}^{\text{A}}\, P_{n-m}(\cos\Delta) = -\overline{\overline{\dot{\mathbf{g}}_{\text{inc}}}}\,\mathbf{T}_{\text{inc}}\,\delta_{n0} \\ \qquad\qquad\qquad\qquad\qquad\qquad\qquad\qquad \text{for } n \in [N_1, N_2], \\ \sum_{m=N_1}^{N_2+1} (-1)^m \overline{\overline{\mathbf{g}_\infty^{n=0}}}\,\mathbf{t}_{nm}^{\text{A}}\, P_{-m-r/k}(-\cos\Delta) = \mathbf{0} \end{cases}$$

where

$$S_v = \begin{vmatrix} 1(v \geq 0) \\ -1(v < 0) \end{vmatrix} \text{ and } \overline{\overline{\dot{\mathbf{g}}_{\text{inc}}}} = -\text{j}p_{\text{inc}}\left(\overline{\overline{\mathbf{G}'_{\text{inc}}}} + {}^{\text{t}}\overline{\overline{\mathbf{G}'_{\text{inc}}}}\right).$$

The matrix $\overline{\overline{\mathbf{g}_\infty^n}}$ is the asymptotic limit of the matrix $\overline{\overline{\mathbf{g}_n}} = -\text{j}p_n(\overline{\overline{\mathbf{G}_n^{\text{A}}}} - \overline{\overline{\mathbf{G}_n^{\text{B}}}})$, i.e.

$$\lim_{|p_n|\to\infty} \overline{\overline{\mathbf{g}_n(p_n)}} = S_{p_n}\,\overline{\overline{\mathbf{g}_\infty^n}}. \tag{A7}$$

For an interface between two elastic media with different properties, $\overline{\overline{\mathbf{g}_\infty^n}}$ is different from the matrix $\overline{\overline{\mathbf{g}_\infty}}$, reported in Danicki (1999) and determined for an interface between identical media. In the case of two different media, it is defined by

$$\overline{\overline{\mathbf{g}_\infty^n}} = \frac{1}{2\omega^2}\begin{bmatrix} X & Y \\ -Y & X \end{bmatrix},$$

where

$$X = \text{j}\left(Z_{\text{A}}k_{\text{S}}^{\text{A}^2} + Z_{\text{B}}k_{\text{S}}^{\text{B}^2}\right),\ Y = S_{p_n}\left(Z_{\text{A}}k_{\text{P}}^{\text{A}^2} - Z_{\text{B}}k_{\text{P}}^{\text{B}^2}\right),$$

$$Z_{\text{A,B}} = \frac{k_{\text{S}}^{\text{A,B}^2}}{\rho_{\text{A,B}}\left(k_{\text{S}}^{\text{A,B}^2} - k_{\text{P}}^{\text{A,B}^2}\right)},$$

$\rho_{\text{A,B}}$ denoting the density of the solids A and B.

The summation limits $m = N_1$ and $m = N_2 + 1$ of the finite series of the system are defined by considering the degree of accuracy that is chosen for the approximation (A7) of $\overline{\overline{\mathbf{g}_n}}$. In the present study, we considered $N_1 = -1$ and $N_2 = 0$. Knowing $\mathbf{T}_{\text{inc}}$, $\mathbf{U}_n^{\text{A,B}}$ and $\mathbf{T}_n^{\text{A,B}}$ are then recovered from the solutions $\mathbf{t}_{nm}^{\text{A}}$ and the relationships (A1)–(A6).